Numerical Experiments with the Osher Upwind Scheme for the Euler Equations

Sukumar R. Chakravarthy*
Stanford University, Stanford, California
and
Stanley Osher†
University of California, Los Angeles, California

The Osher algorithm for solving the Euler equations is an upwind finite difference procedure that is derived by combining the salient features of the theory of conservation laws and the mathematical theory of characteristics for hyperbolic systems of equations. A first-order accurate version of the numerical method was derived by Osher circa 1980 for the one-dimensional non-isentropic Euler equations in Cartesian coordinates. In this paper, the extension of the scheme to arbitrary two-dimensional geometries is explained. Results are then presented for several example problems in one and two dimensions. Future work will include extension of the method to second-order accuracy and the development of implicit time differencing for the Osher algorithm.

Introduction

CONVENTIONAL non-upwind finite difference algorithms have been used extensively to solve a wide variety of problems.[1,2] However, that list of solved problems does not include flows with strong shock waves (say, with upstream Mach numbers of 4.0 and above for the component of velocity normal to the shock) when the shocks are captured. Conventional algorithms are also somewhat unreliable in the sense that for every different problem (and sometimes, every different case in the same class of problems) artificial dissipation terms must be specially tuned and judicially chosen for convergence. Also, complex problems with shocks and steep compression and expansion gradients may defy solution altogether.

Upwind differencing schemes are in general more robust but are also more involved in their derivation and application. Some upwind schemes that have been applied to the Euler equations are Godunov's method,[3,4] Steger and Warming's split flux method,[5] Roe's method,[6] and the split coefficient matrix (SCM) method of the first author of this paper.[7-9] This last SCM method is for the governing equations written in the nonconservation law form. Thus any discontinuities present must be "fitted" for proper application of the SCM method. The first three methods are indeed shock-"capturing" finite difference procedures. In this paper, we refrain from making detailed comparison of the various upwind schemes. The Osher algorithm will be presented for the two-dimensional Euler equations in arbitrary coordinate systems and the results will speak for themselves.

The Osher scheme is an upwind, shock-capturing algorithm. It can be applied to essentially all hyperbolic systems of conservation laws arising in physics, but becomes especially simple for the Euler equations. The method does not require any special properties of the Euler equations such as homogeneity. The Osher scheme is based on a Riemann problem solver, as is Godunov's, but compression waves are used to approximate shocks. This leads to a cleaner and smoother algorithm. The numerical flux functions are written in closed form and include various switches that make the scheme upwind.

We now briefly trace the development of the Osher algorithm for hyperbolic systems. Circa 1980, Engquist and Osher[10-12] developed a monotone upwind scheme for scalar conservation laws and applied it to the small-disturbance equation of transonic flow. The Engquist-Osher algorithm is more robust than the Murman-Cole algorithm in that expansion shocks are eliminated and steady flows are computed more quickly.[13] Osher then developed a generalization of the scalar algorithm for hyperbolic systems of conservation laws.[14] This generalization was further studied by Osher and Solomon.[15] In the work presented in this paper, the Osher algorithm is generalized to arbitrary coordinate systems. This paper explains the algorithm for the two-dimensional Euler equations and discusses results obtained therefrom. In a parallel effort, Osher and Chakravarthy[16] review upwind schemes, present the general three-dimensional Osher scheme in arbitrary coordinate systems, and cover some theoretical nuances of the method. Thus, the last two references[15,16] on the Osher scheme are proffered for review by those readers interested in the method and material presented in this paper.

The rest of this paper is organized as follows: In the next section, the Osher algorithm is presented. The aim here is to clearly state the method, rather than explain the philosophy underlying it. Boundary condition treatment is covered in the

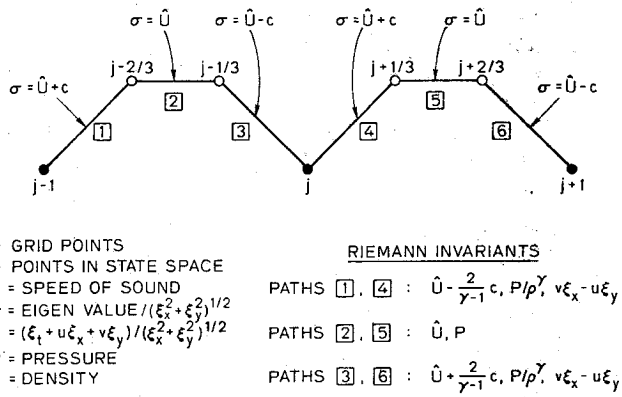

Fig. 1 Schematic representation of Osher scheme in terms of intermediate and grid point values of dependent variables.

Presented as Paper 82-0975 at the AIAA/ASME Third Joint Thermophysics, Fluids, Plasma and Heat Transfer Conference, St. Louis, Mo., June 7-11, 1982; submitted June 11, 1982; revision received Feb. 7, 1983.

*Research Associate, Department of Aeronautics/Astronautics. Member AIAA.
†Professor, Mathematics Department.

succeeding section. Results are presented in the last section. These include examples from one-dimensional flow, quasi-one-dimensional Laval nozzle flow, conical supersonic flow past a wedge airfoil, and Mach 8 supersonic flow past a circular cylinder. The quality of the results is expected to prove the method's worth.

The Osher Scheme

Euler Equations

The two-dimensional Euler equations may be written in conservation law form in Cartesian coordinates as

$$Q_t + E_x + F_y = 0 \tag{1}$$

where

$$Q = \begin{bmatrix} \rho \\ \rho u \\ \rho v \\ e \end{bmatrix}, \quad E = \begin{bmatrix} \rho u \\ \rho u^2 + p \\ \rho uv \\ (e+p)u \end{bmatrix}, \quad F = \begin{bmatrix} \rho v \\ \rho vu \\ \rho v^2 + p \\ (e+p)v \end{bmatrix} \tag{2}$$

In the above, the Cartesian coordinates are denoted by x and y and the corresponding velocity components are u and v. Time is denoted by t, pressure by p, and density by ρ. The total energy per unit volume is denoted by e and is given by $e = p/(\gamma-1) + \rho(u^2+v^2)/2$ where γ is the ratio of specific heats.

We make an arbitrary change of independent variables of the form

$$\tau = t, \quad \xi = \xi(t,x,y), \quad \eta = \eta(t,x,y) \tag{3}$$

The governing Euler equations may then be transformed by chain-rule differentiation into

$$Q_\tau + (\xi_t Q_\xi + \xi_x E_\xi + \xi_y F_\xi) + (\eta_t Q_\eta + \eta_x E_\eta + \eta_y F_\eta) = 0 \tag{4}$$

For later use, we define

$$\hat{E} = \xi_t Q + \xi_x E + \xi_y F = \hat{E}(\xi, Q)$$

$$\hat{F} = \eta_t Q + \eta_x E + \eta_y F = \hat{F}(\eta, Q) \tag{5}$$

where $\hat{E}(\xi,Q)$ denotes the dependence of $\hat{E}$ on ξ_t, ξ_x, ξ_y and Q, $E(Q)$, $F(Q)$.

Eigenvalues and Eigenvectors

If we define Jacobian matrices $A = \partial E/\partial Q$ and $B = \partial F/\partial Q$, the governing Euler equations (4) may be rewritten in the quasilinear form

$$Q_\tau + (\xi_t I + \xi_x A + \xi_y B) Q_\xi + (\eta_t I + \eta_x A + \eta_y B) Q_\eta = 0 \tag{6}$$

where I is the identity matrix. In the mathematical theory of characteristics of hyperbolic systems of equations, we are interested in the eigenvalues and eigenvectors of the coefficient matrices

$$\hat{A} = \xi_t I + \xi_x A + \xi_y B, \quad \hat{B} = \eta_t I + \eta_x A + \eta_y B \tag{7}$$

Before defining the eigenvalues, we define normalized metrics (shown for only ξ terms for brevity)

$$k_0 = \xi_t/k_n, \quad k_1 = \xi_x/k_n, \quad k_2 = \xi_y/k_n \tag{8}$$

where $k_n = \sqrt{\xi_x^2 + \xi_y^2}$. Then, if the speed of sound is denoted by $c = (\gamma p/\rho)^{1/2}$ the eigenvalues of $\hat{A}$ are

$$\lambda_1 = (\hat{U}+c)k_n, \quad \lambda_{2,3} = \hat{U}k_n, \quad \lambda_4 = (\hat{U}-c)k_n \tag{9}$$

where $\hat{U} = k_0 + k_1 u + k_2 v$.

The right or column eigenvectors of the coefficient matrix $\hat{A}$ written in the same order as the eigenvalues and denoted by $r_1 = r(\lambda_1)$, etc., may be written as follows to constitute the columns of a matrix:

$R =$

r_1	r_2	r_3	r_4
ρ/c	ρ/c	ρ/c	ρ/c
$u\rho/c + k_1\rho$	$u\rho/c + k_2\rho$	$u\rho/c - k_2\rho$	$u\rho/c - k_1\rho$
$v\rho/c + k_2\rho$	$v\rho/c - k_1\rho$	$v\rho/c + k_1\rho$	$v\rho/c - k_2\rho$
$\frac{(u^2+v^2)\rho}{2c} + \rho u k_1 + \rho v k_2 + \frac{\rho c}{(\gamma-1)}$	$\frac{(u^2+v^2)\rho}{2c} + \rho u k_2 - \rho v k_1$	$\frac{(u^2+v^2)\rho}{2c} - \rho u k_2 + \rho v k_1$	$\frac{(u^2+v^2)\rho}{2c} - \rho u k_1 - \rho v k_2 + \frac{\rho c}{(\gamma-1)}$

(10)

The eigenvalues and eigenvectors of $\hat{B}$ are easily obtained from those of $\hat{A}$ by just substituting η for ξ.

Riemann Invariants

Riemann invariants are the building blocks for the Osher algorithm applied to Euler equations. Riemann invariants are associated with the eigenvalues of the coefficient matrices and are obtained from the corresponding right eigenvectors. For the Osher scheme, the Riemann invariants ψ corresponding to the ℓth eigenvalue are obtained by solving (see Ref. 15 for details of the one-dimensional case),

$$\nabla_Q \psi \cdot r_\ell(Q) = 0 \tag{11}$$

where ∇_Q is the gradient operator with respect to the vector of dependent variables denoted in Eq. (2) by Q.

It may easily be verified that the following are Riemann invariants:

for $\lambda_1 = (\hat{U}+c)k_n$

$$\psi_2^1 = \hat{U} - 2c/(\gamma-1)$$

$$\psi_3^1 = p/\rho^\gamma = S = \text{entropy}$$

$$\psi_4^1 = vk_1 - uk_2 = \hat{V} \tag{12a}$$

for $\lambda_{2,3} = \hat{U}k_n$

$$\psi_1^{2,3} = p, \qquad \psi_4^{2,3} = \hat{U} \tag{12b}$$

for $\lambda_4 = (\hat{U}-c)k_n$

$$\psi_1^4 = \hat{U} + 2c/(\gamma-1)$$

$$\psi_2^4 = p/\rho^\gamma S = \text{entropy}$$

$$\psi_3^4 = vk_1 - uk_2 = \hat{V} \tag{12c}$$

In the above, the superscript denotes the appropriate eigenvalue to which the Riemann invariants correspond and the notation is consistent with Ref. 15.

Intermediate States

Thus far, we have been describing general theoretical properties of the governing Euler equations. We now begin looking at the Osher algorithm as a finite difference scheme.

In a finite difference scheme, the variables of interest are defined at grid points

$$\xi_j, \quad j=1,\ldots,j_{\max}, \quad \eta_k, \quad k=1,\ldots,k_{\max}$$

Grid point values of the dependent variable Q are denoted by $Q_{j,k}=Q(\xi_j,\eta_k)$. Let us consider the ξ coordinate in detail and to simplify our notation, we suppress the η index k.

Conventional finite difference schemes utilize the grid point values of the dependent values in a simple manner. The derivative E_ξ would for example be computed as $E_\xi \approx (E_{j+1}-E_{j-1})/(2\Delta\xi)$. The Osher algorithm is somewhat more sophisticated. Fundamental to the Osher scheme are intermediate states of the dependent variables, which are defined between their state values at the grid points. While grid point values are defined by Q_{j-1}, Q_j, etc., the corresponding intermediate states are defined by $Q_{j-2/3}$ and $Q_{j-1/3}$. The rest of this section describes how these intermediate values are defined and their significance.

Figure 1 serves as a guide to the construction of the intermediate states. We connect the states at $j-1$ and j through a curve in state space which is made up of three subpaths. The first path connects Q_{j-1} to $Q_{j-2/3}$ and is associated with λ_1. Path 2 connecting $Q_{j-2/3}$ to $Q_{j-1/3}$ is associated with $\lambda_{2,3}$ and path 3 connecting $Q_{j-1/3}$ and Q_j is associated with λ_4. If s is the running coordinate along these paths, we choose

$$\left(\frac{dQ}{ds}\right)_1 = r_1(Q)$$

$$\left(\frac{dQ}{ds}\right)_2 = r_{2,3}(Q)$$

$$\left(\frac{dQ}{ds}\right)_3 = r_4(Q) \tag{13}$$

From the definition of the Riemann invariants in Eq. (11), it is clear that along each subpath ℓ

$$\frac{d\psi}{ds} = \nabla_Q \psi^\ell \cdot r_\ell = 0 \tag{14}$$

Thus, we verify the appropriateness of the name Riemann "invariants" that we ascribed to ψ.

Thus $\psi^1_{2,3,4}$ are constant between Q_{j-1} and $Q_{j-2/3}$; $\psi^{2,3}_{1,4}$ are constant between $Q_{j-2/3}$ and $Q_{j-1/3}$; $\psi^4_{1,2,3}$ are constant between $Q_{j-1/3}$ and Q_j. Equating Riemann invariants between the end points of each subpath we obtain $3+2+3=8$ equations to obtain the 8 unknown values of $Q_{j-2/3}$ and $Q_{j-1/3}$ from the known values at Q_{j-1} and Q_j. Thus the dependent variables at $j-2/3$ and $j-1/3$ are defined by the following formulas:

$$\rho^{(\gamma-1)/2}_{j-1/3} = \frac{[(\gamma-1)(\hat{U}_j-\hat{U}_{j-1})/2+c_j+c_{j-1}]}{\{c_j[1+(S_{j-1}/S_j)^{1/(2\gamma)}]\}}\rho^{(\gamma-1)/2}_j \tag{15a}$$

$$\rho^{(\gamma-1)/2}_{j-2/3} = \frac{[(\gamma-1)(\hat{U}_j-\hat{U}_{j-1})/2+c_j+c_{j-1}]}{\{c_{j-1}[1+(S_j/S_{j-1})^{1/(2\gamma)}]\}}\rho^{(\gamma-1)/2}_{j-1} \tag{15b}$$

$$p_{j-2/3} = p_{j-1/3} = S_{j-1}\rho^\gamma_{j-2/3} \tag{15c}$$

$$\hat{U}_{j-2/3} = \hat{U}_{j-1} - \frac{2}{(\gamma-1)}(c_{j-1}-c_{j-2/3})$$

$$= \hat{U}_{j-1/3} = \hat{U}_j + \frac{2}{(\gamma-1)}(c_j-c_{j-1/3}) \tag{15d}$$

$$\hat{V}_{j-2/3} = \hat{V}_{j-1} \tag{15e}$$

$$\hat{V}_{j-1/3} = \hat{V}_j \tag{15f}$$

Once $Q_{j-1/3}$ and $Q_{j-2/3}$ are known, λ_1 may be computed at $j-1$ and $j-2/3$ and λ_4 at j and $j-1/3$. It can be shown that λ_1 and λ_4 can at most change sign only once along paths 1 and 3, respectively. If these eigenvalues do indeed change sign [if $\lambda_1(j-1)\cdot\lambda_1(j-2/3)<0$, for example], it becomes necessary to compute the dependent variables at the point along paths 1 and 4 where the respective eigenvalues λ_1 and λ_4 vanish. These "sonic" points are defined as $\underline{Q}_{j-2/3}$ and $\underline{Q}_{j-1/3}$ (with the underscore) and are given by the formulas that follow. In order to obtain $\underline{Q}_{j-2/3}$, for example, we make use of Eqs. (12a) equated between $j-1$ and the sonic point before $j-2/3$ along with $\underline{\hat{U}}+\underline{c}=0$ ("sonic" condition) to yield four equations for the four unknowns $\underline{Q}_{j-2/3}$:

$$\underline{\hat{U}}_{j-1/3} = \left(\frac{\gamma-1}{\gamma+1}\right)\left(\hat{U}_j + \frac{2}{(\gamma-1)}c_j\right) \tag{16a}$$

$$\underline{\rho}^{(\gamma-1)/2}_{j-1/3} = \underline{\hat{U}}_{j-1/3}/(\gamma S_j)^{1/2} \tag{16b}$$

$$\underline{p}_{j-1/3} = S_j\underline{\rho}^\gamma_{j-1/3} \tag{16c}$$

$$\underline{\hat{V}}_{j-1/3} = \hat{V}_j \tag{16d}$$

$$\underline{\hat{U}}_{j-2/3} = \left(\frac{\gamma-1}{\gamma+1}\right)\left(\hat{U}_{j-1} - \frac{2}{(\gamma-1)}c_{j-1}\right) \tag{16e}$$

$$\underline{\rho}^{(\gamma-1)/2}_{j-2/3} = -\underline{\hat{U}}_{j-2/3}/(\gamma S_{j-1})^{1/2} \tag{16f}$$

$$\underline{p}_{j-2/3} = S_{j-1}\underline{\rho}^\gamma_{j-2/3} \tag{16g}$$

$$\underline{\hat{V}}_{j-2/3} = \hat{V}_{j-1} \tag{16h}$$

Along path 2, the Riemann invariant $\psi^{2,3}_4 = \lambda_2/k_n$. Thus λ_2 does not change either magnitude or sign. Incidentally, the λ_1 and λ_4 fields are called genuinely nonlinear and the field corresponding to $\lambda_{2,3}$ is termed linearly degenerate.

In Eqs. (15) and (16), it is straightforward to decode for u, v from $\hat{U}$, $\hat{V}$ from the definition of the contravariant velocities. It is very interesting to compare the Riemann invariants of the one-dimensional equations given in Ref. 15 and those given here for arbitrary coordinate systems. For $\psi^1_{2,3}$ and $\psi^4_{1,2}$, which are present for both one and two dimensions, just substituting $\hat{U}$ for u in Ref. 15 results in the Riemann invariants given here. Thus the formulas given by Eqs. (15) and (16) may also be obtained from Ref. 15 by substituting $\hat{U}$ for u. We do have more Riemann invariants (ψ^1_4 and ψ^4_3) for the two-dimensional case with four dependent variables than for the one-dimensional case with only three dependent variables. This extra Riemann invariant appearing for paths 1 and 3 is $\hat{V}=vk_1-uk_2$, suggesting the obvious extension to three-dimensional problems, the theory for which is covered in Ref. 16.

Paths of Integration

We now explain how the intermediate state values and grid point values of the dependent variables are utilized to form Osher's algorithm for the Euler equations. We begin by approximating the spatial derivative terms of Eq. (4) as follows (as usual, considering only the ξ terms in detail),

$$\xi_t Q_\xi + \xi_x E_\xi + \xi_y F_\xi$$

$$\approx \left(\frac{1}{\Delta\xi}\right)\left[\int_{Q_{j-1}}^{Q_j} X\hat{A}\,dQ + \int_{Q_j}^{Q_{j+1}} (I-X)\hat{A}\,dQ\right] \tag{17}$$

The matrix $X(Q)$ and the paths of integration are what define the scheme. The integration subpaths have already been defined (curves 1-3 of Fig. 1). The matrix $X(Q)$ is defined to be

$$X(Q) = R(Q)\,\mathrm{diag}\{\tfrac{1}{2}+\tfrac{1}{2}\mathrm{sign}[\lambda_\ell(Q)]\}R^{-1}(Q) \tag{18}$$

where λ_i were defined by Eq. (9) and the columns of R in Eq. (10). Thus

$$X\hat{A} = R\,\mathrm{diag}\{\max(\lambda_i, 0)\}R^{-1} = \hat{A}^+$$

$$(I-X)\hat{A} = R\,\mathrm{diag}\{\min(\lambda_i, 0)\}R^{-1} = \hat{A}^- \tag{19}$$

The upwind flavor of the scheme becomes apparent from this.

Equation (17) may be further simplified by breaking up the integration over the subpaths of integration,

$$\int_{Q_{j-1}}^{Q_j} \hat{A}^+ \mathrm{d}Q + \int_{Q_j}^{Q_{j+1}} \hat{A}^- \mathrm{d}Q = \hat{E}(\xi, Q_{j+1}) - \hat{E}(\xi, Q_j)$$
$$+ \int_{j-1}^{j-2/3} \hat{A}^+ \left(\frac{\mathrm{d}Q}{\mathrm{d}s}\right)_1 \mathrm{d}s + \int_{j-2/3}^{j-1/3} \hat{A}^+ \left(\frac{\mathrm{d}Q}{\mathrm{d}s}\right)_2 \mathrm{d}s$$
$$+ \int_{j-1/3}^{j} \hat{A}^+ \left(\frac{\mathrm{d}Q}{\mathrm{d}s}\right)_3 \mathrm{d}s - \int_{j}^{j+1/3} \hat{A}^+ \left(\frac{\mathrm{d}Q}{\mathrm{d}s}\right)_4 \mathrm{d}s$$
$$- \int_{j+1/3}^{j+2/3} \hat{A}^+ \left(\frac{\mathrm{d}Q}{\mathrm{d}s}\right)_5 \mathrm{d}s - \int_{j+2/3}^{j+1} \hat{A}^+ \left(\frac{\mathrm{d}Q}{\mathrm{d}s}\right)_6 \mathrm{d}s \tag{20}$$

It is obvious then that the building blocks are the subintegrals along the subpaths connecting every pair of neighboring points. Let us consider for example the pair of points $j-1$ and j. We define

$$D_1 = \int_{Q_{j-1}}^{Q_{j-2/3}} \hat{A}^+ \mathrm{d}Q$$

$$D_2 = \int_{Q_{j-2/3}}^{Q_{j-1/3}} \hat{A}^+ \mathrm{d}Q$$

$$D_3 = \int_{Q_{j-1/3}}^{Q_j} \hat{A}^+ \mathrm{d}Q \tag{21}$$

While the integration formulas shown in the above equations seem formidable to evaluate, they simplify greatly and each subintegral actually reduces to a difference of the fluxes $\hat{E}(\xi, Q)$ at the grid, intermediate, or sonic points. Thus

$$D_1 = \hat{E}(\xi, Q_{j-2/3}) - \hat{E}(\xi, Q_{j-1})$$
$$\text{if } \lambda_1(Q_{j-1}) > 0 \text{ and } \lambda_1(Q_{j-2/3}) > 0$$
$$= \hat{E}(\xi, Q_{j-2/3}) - \hat{E}(\xi, Q_{j-2/3})$$
$$\text{if } \lambda_1(Q_{j-1}) \le 0 \text{ and } \lambda_1(Q_{j-2/3}) > 0$$
$$= \hat{E}(\xi, Q_{j-2/3}) - \hat{E}(\xi, Q_{j-1})$$
$$\text{if } \lambda_1(Q_{j-1}) > 0 \text{ and } \lambda_1(Q_{j-2/3}) \le 0$$
$$= 0$$
$$\text{if } \lambda_1(Q_{j-1}) \le 0 \text{ and } \lambda_1(Q_{j-2/3}) \le 0 \tag{22}$$

$$D_2 = \hat{E}(\xi, Q_{j-1/3}) - \hat{E}(\xi, Q_{j-2/3}) \quad \text{if } \lambda_{2,3}(Q_{j-1/3}) > 0$$
$$= 0$$
$$\text{if } \lambda_{2,3}(Q_{j-1/3}) \le 0 \tag{23}$$

$$D_3 = \hat{E}(\xi, Q_j) - \hat{E}(\xi, Q_{j-1/3})$$
$$\text{if } \lambda_4(Q_{j-2/3}) > 0 \text{ and } \lambda_4(Q_j) > 0$$
$$= \hat{E}(\xi, Q_j) - \hat{E}(\xi, Q_{j-1/3})$$
$$\text{if } \lambda_4(Q_{j-1/3}) \le 0 \text{ and } \lambda_4(Q_j) > 0$$
$$= \hat{E}(\xi, Q_{j-1/3}) - \hat{E}(\xi, Q_{j-1/3})$$
$$\text{if } \lambda_4(Q_{j-1/3}) > 0 \text{ and } \lambda_4(Q_j) \le 0$$
$$= 0$$
$$\text{if } \lambda_4(Q_{j-1/3}) \le 0 \text{ and } \lambda_4(Q_j) \le 0 \tag{24}$$

The Osher Scheme

The entire algorithm to update the dependent variables at a grid point j from a time level n to the next level $n+1$ can thus be simply written as a concise sequence of steps:

ξ terms—

1) Evaluate dependent variables at intermediate points between $j-1$ and j using Eqs. (15).

2) Using Eqs. (16) evaluate those sonic points that occur between $j-1$ and j (if the eigenvalues change sign).

3) Evaluate subintegrals D_1, D_2, D_3 between grid points $j-1$ and j using Eqs. (22-24). Fluxes $\hat{E}$ at grid points and intermediate points are evaluated as needed.

4) Repeat steps 1-3 between grid points j and $j+1$.

5) Substitute subintegrals and fluxes into Eq. (20) to evaluate the ξ terms.

η terms—

6) Repeat steps 1-5 for the η terms (formulas for η obtained by substituting η for ξ in the formulas for the ξ terms).

Update—

7) Update dependent variables using

$$Q_{j,k}^{n+1} = Q_{j,k}^n - \frac{\Delta\tau}{\Delta\xi}\left[\int_{Q_{j-1,k}}^{Q_{j,k}} \hat{A}^+ \mathrm{d}Q + \int_{Q_{j,k}}^{Q_{j+1,k}} \hat{A}^- \mathrm{d}Q\right]$$
$$- \frac{\Delta\tau}{\Delta\eta}\left[\int_{Q_{j,k-1}}^{Q_{j,k}} \hat{B}^+ \mathrm{d}Q + \int_{Q_{j,k}}^{Q_{j,k+1}} \hat{B}^- \mathrm{d}Q\right] \tag{25}$$

with the terms multiplied by $\Delta\tau$ having been evaluated in steps 1-6.

Method Variations

In the above, the point at which the metrics were to be evaluated was intentionally kept general. In other words, in evaluating $\hat{E}(\xi, Q)$, we were explicit in stating what values of Q (e.g., Q_{j-1}, $Q_{j-2/3}$, $Q_{j-1/3}$, Q_j, $Q_{j-1/3}$, $Q_{j-2/3}$) were to be used. However, the values that ξ_t, ξ_x, ξ_y must take were not specified. Depending on what values these metrics take, we define two versions of the Osher algorithm.

Method 1

For the first method, when dependent variables at a grid point j, k are being updated, we define

$$\hat{E}(\xi, Q) = \hat{E}(\xi_j, Q), \quad \hat{F}(\eta, Q) = \hat{F}(\eta_k, Q) \tag{26}$$

This method is simply based on the chain rule form of the equations.

Method 2

For the second method based on a "variable coefficient" conservation upwind scheme idea of Abrahamsson and Osher,[17] the dependence of the fluxes on the metrics is defined to be

$$\hat{E}(\xi, Q) = \hat{E}(\xi_{j-1/2}, Q) \quad \text{in evaluating } \int_{Q_{j-1}}^{Q_j} \hat{A}^+ \mathrm{d}Q$$

$$\hat{E}(\xi, Q) = \hat{E}(\xi_{j+1/2}, Q) \quad \text{in evaluating } \int_{Q_j}^{Q_{j+1}} \hat{A}^- \mathrm{d}Q \tag{27}$$

and similarly for $\hat{F}(\eta,Q)$. Compared to method 1, method 2 requires only about half the computations for every step. This is because

$$\int_{Q_{j-1}}^{Q_j} \hat{A}^+(\xi_{j-1/2},Q)\,dQ + \int_{Q_j}^{Q_{j+1}} \hat{A}^-(\xi_{j+1/2},Q)\,dQ$$
$$= \hat{E}(\xi_{j+1/2},Q_{j+1}) - \hat{E}(\xi_{j+1/2},Q_j)$$
$$+ \int_{Q_{j-1}}^{Q_j} \hat{A}^+(\xi_{j-1/2},Q)\,dQ - \int_{Q_j}^{Q_{j+1}} \hat{A}^+(\xi_{j+1/2},Q)\,dQ$$
Term 1 Term 2 (28)

with term 1, which is used to advance values at j, being equal to term 2, used to advance the previous point. This telescoping property can be exploited so that, but for the first grid point, only one of the two terms 1 or 2 need be computed. For this and other reasons, we prefer method 2. Method 2 may also be obtained from the "weak" conservation law form. More information on these and one more variation is given in Ref. 16.

Variations in Ordering

Other variations to the basic algorithm are possible. These new modifications are based on the order in which the eigenvalues were associated with the three subpaths linking Q_{j-1} and Q_j. Until now, we have presented $\hat{U}+c$, $\hat{U}$, $\hat{U}-c$ to correspond to paths Q_{j-1} to $Q_{j-2/3}$, $Q_{j-2/3}$ to $Q_{j-1/3}$, $Q_{j-1/3}$ to Q_j for good reason. This ordering would result in an exact resolution of the steady discontinuities[15] with at most two transition points (for a grid aligned with the discontinuity in two and three dimensions) without any overshoots. It was indicated in Ref. 15 that proving this property would be difficult for other orderings of the paths. However, numerical evidence for the ordering $\hat{U}-c$, $\hat{U}$, $\hat{U}+c$ to correspond to Q_{j-1} to $Q_{j-2/3}$, $Q_{j-2/3}$ to $Q_{j-1/3}$, $Q_{j-1/3}$ to Q_j has been quite encouraging and will be further investigated in future work.

Boundary Conditions

We discuss in this section the numerical implementation of boundary conditions. We present a treatment that uses the Riemann invariants introduced in the previous section. We refer the interested reader to Ref. 16 for a boundary point treatment slightly different from what is presented here.

Discretization at Boundaries

Let us look at the ξ-derivative terms in detail. The Osher algorithm for interior points may be represented by

$$Q_j^{n+1} = Q_j^n - \frac{\Delta\tau}{\Delta\xi}\left(\int_{Q_{j-1}}^{Q_j} \hat{A}^+\,dQ + \int_{Q_j}^{Q_{j+1}} \hat{A}^-\,dQ\right) - \frac{\Delta\tau}{\Delta\eta}(\eta-\text{terms}) \quad (29)$$

The problem at the extremes of ξ is that one of the integrals in the above equation cannot be evaluated. The "+" part is undefined at the left boundary and the "−" part undefined at the right boundary. The approach we take is to first update Q_j at the boundary points using only the integrals that are defined. For example, at the left extremity of the grid, we use

$$Q_j = Q_j^n - \frac{\Delta\tau}{\Delta\xi}\left(\int_{Q_j}^{Q_{j+1}} \hat{A}^-\,dQ\right) + \ldots \quad (30)$$

This updated value is referred to as the predicted value and denoted by superscript ( )*. This prediction equation, when coupled with the interior point equation, can be shown to satisfy the difference analog of global conservation. The predicted value is then corrected to account for the boundary condition(s) that otherwise would not be satisfied. This last step uses the influence of the appropriate wave(s): the right-moving wave(s) at the left boundary and the left-moving wave(s) at the right boundary. The actual mechanics of doing that for two boundary conditions (needed for the results in the next section) are described below.

Subsonic Outflow

In the Laval nozzle example to be shown in the next section, the exit pressure (back pressure) is chosen so that a shock divides a supersonic oncoming flow from a subsonic outflow. For this one-dimensional example, the characteristic velocities (eigenvalues of the Jacobian matrix) are $u+c$, u, $u-c$. With flow from left to right, it is the third eigenvalue $u-c$ that is negative at the subsonic outflow boundary. The influence of this inward propagation cannot be properly accounted for by the difference formulas

$$Q_j^* = Q_j^n - \frac{\Delta\tau}{\Delta\xi}\left(\int_{Q_{j-1}}^{Q_j} \hat{A}^+\,dQ\right) + \ldots \quad (31)$$

Along the $u-c$ characteristic, the Riemann invariants imply

$$\left(u^* + \frac{2}{\gamma-1}c^*\right) = \left(u^{n+1} + \frac{2}{\gamma-1}c^{n+1}\right)$$
$$\frac{p^*}{(\rho^*)^\gamma} = \frac{p^{n+1}}{(\rho^{n+1})^\gamma} \quad (32a)$$

These give us only two equations to solve for the three unknowns u^{n+1}, p^{n+1}, and ρ^{n+1}. Thus, we supplement Eq. (32a) with the boundary condition

$$p^{n+1} = p_{\text{exit}} = \text{given} \quad (32b)$$

and proceed to solve for Q^{n+1}.

Surface Tangency

The supersonic flow past a circular cylinder is a two-dimensional problem for which results are presented in the next section. At the surface of the cylinder, flow tangency requires that

$$\hat{U} = 0 \quad (33)$$

Assuming that the cylinder forms a lower boundary, we find that the influence of the $(\hat{U}+c)k_n$ characteristic cannot be properly accounted for at the boundary by a difference formula such as Eq. (30). However, we know that Riemann invariants along the $(\hat{U}+c)k_n$ characteristic imply

$$\left(\hat{U}^* - \frac{2}{\gamma-1}c^*\right) = \left(\hat{U}^{n+1} - \frac{2}{\gamma-1}c^{n+1}\right)$$
$$\frac{p^*}{(\rho^*)^\gamma} = \frac{p^{n+1}}{(\rho^{n+1})^\gamma}$$
$$\hat{V}^* = \hat{V}^{n+1} \quad (34a)$$

Coupled with the boundary conditions

$$\hat{U}^{n+1} = 0 \quad (34b)$$

we have four equations for the four unknowns $(\rho,u,v,p)^{n+1}$ and we can proceed to solve for Q^{n+1}.

Results

Constant Area Duct

The first example presented in this section is the flow through a constant area duct which is described by the Euler

Table 1 Steady shock in a constant-area duct

	M_{inflow}	ρ	u	p	$\ln(p/\rho^\gamma)$	$u+\frac{2c}{\gamma-1}$	$u-\frac{2c}{\gamma-1}$
Left of shock transition	2.0	0.10000E1	0.23664E1	0.10000E1	0.00000E0	0.82825E1	−0.35496E1
	1000.0	0.10000E1	0.11832E4	0.10000E1	0.00000E0	0.11891E4	0.11773E4
First shock transition point	2.0	0.13434E1	0.19013E1	0.16741E1	0.10196E0	0.85055E1	−0.47028E1
	1000.0	0.22694E1	0.67973E3	0.27797E6	0.11388E2	0.27502E4	−0.13907E4
Second shock transition point	2.0	0.25158E1	0.97642E0	0.41476E1	0.13092E0	0.85726E1	−0.66198E1
	1000.0	0.57403E1	0.22018E3	0.10966E7	0.11461E2	0.28060E4	−0.23656E4
Right of shock transition	2.0	0.26667E1	0.88741E1	0.45000E1	0.13092E0	0.85726E1	−0.67978E1
	1000.0	0.59999E1	0.19720E3	0.11667E7	0.11461E2	0.28060E4	−0.24116E4

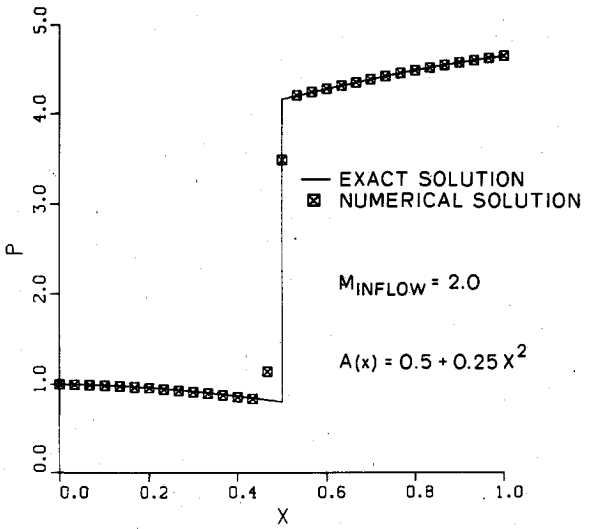

Fig. 2 Pressure distribution along quasi-one-dimensional Laval nozzle.

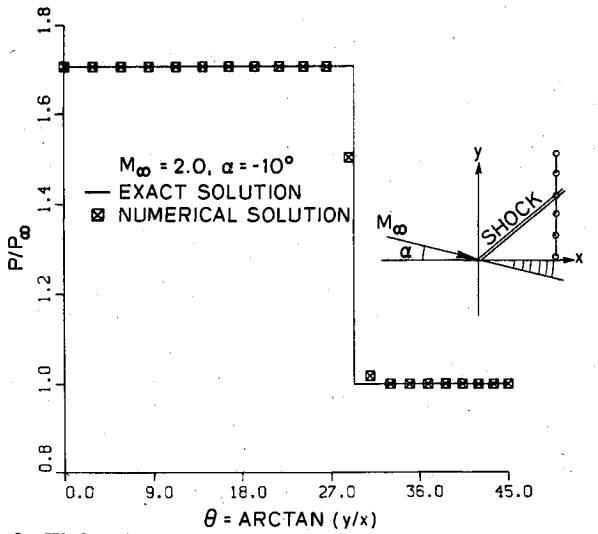

Fig. 3 Wedge in supersonic flow with attached shock wave ($M_\infty = 2.0$, $\alpha = -10$ deg).

equations

$$\begin{bmatrix}\rho\\ \rho u\\ e\end{bmatrix}_t + \begin{bmatrix}\rho u\\ \rho u^2+p\\ (e+p)u\end{bmatrix}_x = 0 \tag{35}$$

Let a steady shock wave separate two constant states in such a duct. The numerical solution obtained using the Osher scheme applied to one-dimensional flow[15] will show that the shock is represented by two transition points that lie between the left and right constant states. Table 1 summarizes the results for two inflow Mach numbers, 2.0 and 1000.0. The numerical solution at grid points to the left of the two transition points agrees exactly (up to computer precision) with the prescribed upstream values. At all grid points to the right, the solution matches exactly with the analytic solution for a steady shock wave for the prescribed upstream Mach number. The sharpness of the transition is evident for both Mach 2 and 1000 and it is a monotone transition for both cases as predicted by theory.[15] The shock in this case corresponds to the field of the eigenvalue $u-c$ and it is interesting also to note that the corresponding Riemann invariants $u+2c/(\gamma-1)$ and S actually have a one-point transition at the shock.

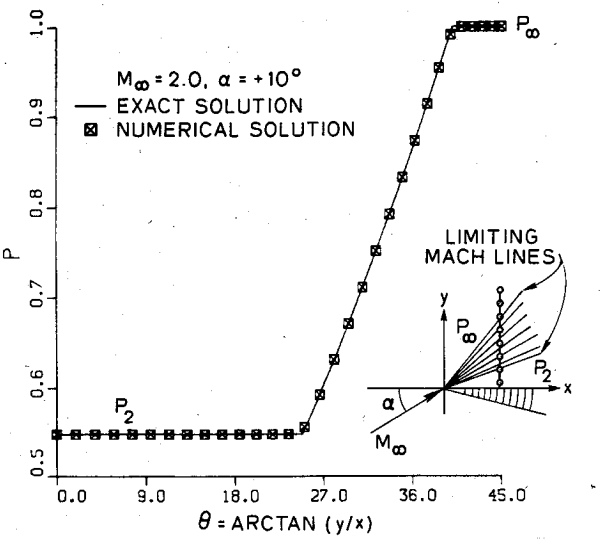

Fig. 4 Wedge in supersonic flow with expansion fan ($M_\infty = 2.0$, $\alpha = +10$ deg).

Laval Nozzle

The next example is the flow through a quasi-one-dimensional Laval nozzle with a prescribed area variation along the axis of the duct. The governing equations are

$$Q_t + E_x + \left(\frac{\delta A/\delta x}{A}\right)H = 0 \tag{36}$$

with Q and E defined in Eq. (35) and

$$H = \begin{bmatrix}\rho u\\ \rho u^2\\ (e+p)u\end{bmatrix}$$

The area distribution was chosen to be

$$A(x) = y_{\min} + (y_{\max} - y_{\min})x^2 \qquad 0 \le x \le 1.0 \tag{37}$$

with $y_{\max} = 0.75$ and $y_{\min} = 0.5$.

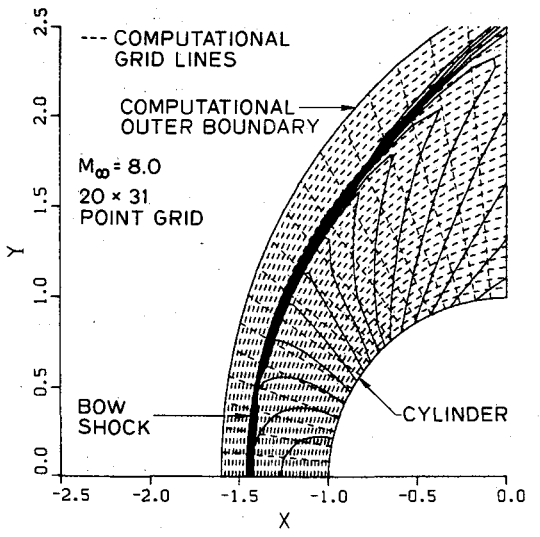

Fig. 5 Pressure contours about a circular cylinder in a supersonic flow of $M_\infty = 8.0$.

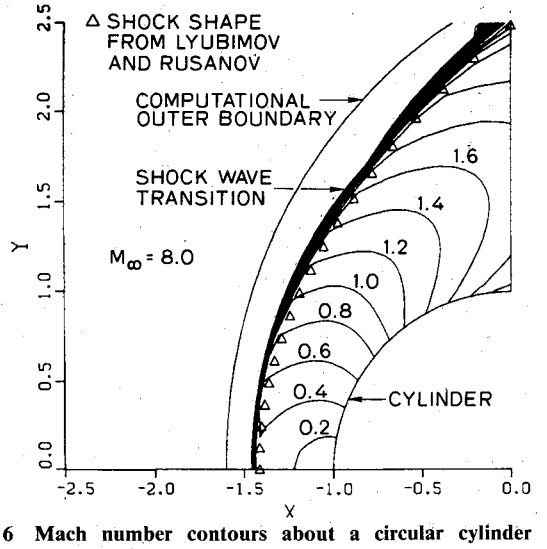

Fig. 6 Mach number contours about a circular cylinder in a supersonic flow of $M_\infty = 8.0$.

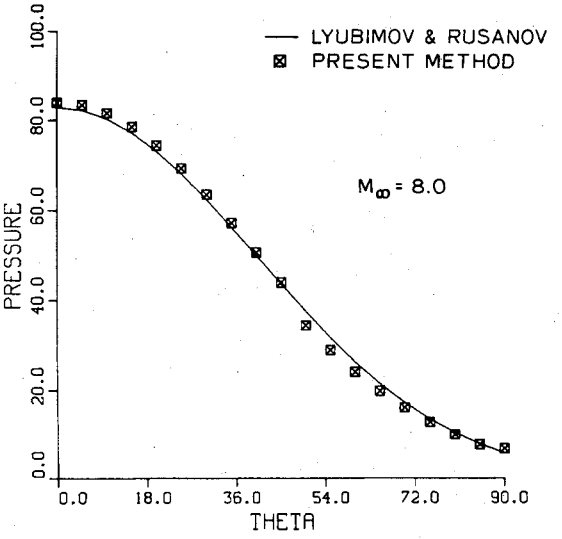

Fig. 7 Surface pressure distribution over a circular cylinder in supersonic stream with $M_\infty = 8.0$.

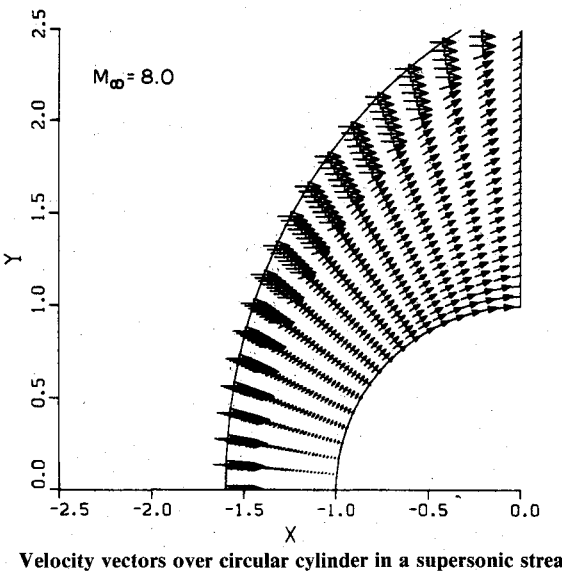

Fig. 8 Velocity vectors over circular cylinder in a supersonic stream with $M_\infty = 8.0$.

This example requires the use of the subsonic outflow boundary condition covered in the last section. The back pressure was so chosen that a shock was situated at $x = 0.5$. The inflow was prescribed to be supersonic. For an inflow Mach number of 2.0, the numerically obtained (Osher scheme) pressure distribution is compared with the exact solution in Fig. 2. Excellent agreement is evident along with the sharp two-point shock transition.

Supersonic Flow Past a Wedge

The third example considered is the supersonic flow past a wedge. The wedge surface is laid out aligned with the x axis with the freestream flow inclined to this surface. For negative incidence α, a straight oblique shock attached to the leading edge of the wedge must result. For positive α, a Prandtl-Meyer expansion fan centered at the leading edge must occur. This example requires the use of coordinate transformations in our chosen way of obtaining a solution. If we transform the independent variables with

$$\tau = t, \quad \xi = x, \quad \eta = y/x \tag{38}$$

we can set the variations of the dependent variables with respect to ξ to be zero by similarity. Thus the analysis of this problem requires only one spatial dimension η along with time τ. Results are now presented for a freestream Mach number of 2.0. Method 2 of the previous section was utilized for these examples.

First, we compare the numerical and exact solutions for $\alpha = -10$ deg where the oblique shock is situated at approximately 30 deg from the wedge surface. Figure 3 shows the excellent agreement for this case. Next, we consider $\alpha = +10$ deg in Fig. 4. Once again, superior agreement between the numerical and exact solutions is clearly seen. The excellent behavior of the numerical solution near the points of slope discontinuity in the pressure distribution is also obvious. The absence of any oscillations or smearing offers proof of the superior abilities of the numerical method.

Supersonic Flow Past a Cylinder

Finally, we turn our attention to the fully two-dimensional flow past a circular cylinder with a freestream Mach number of 8.0. The computational domain was chosen to include the bow shock in its interior and the shock was "captured" as in the previous examples. Grid lines were constructed by first choosing an outer boundary shape, drawing radial lines at equiangular increments, and drawing the other family of lines to be equally spaced between the cylinder and the outer boundary. The calculations were started "impulsively" by

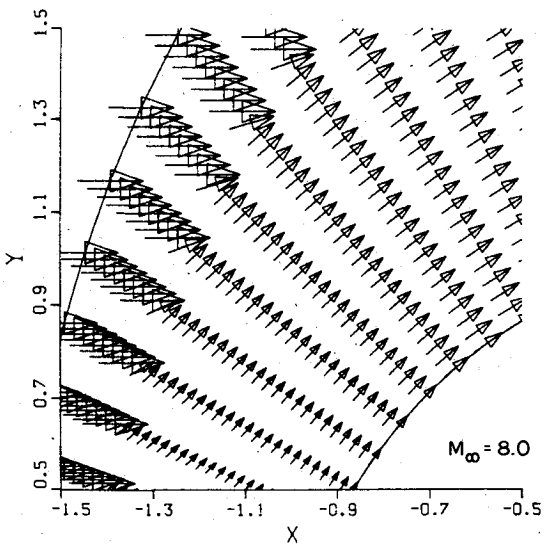

Fig. 9 Closeup of velocity vector field shown in Fig. 8.

Table 2 Computational time comparisons

Computer	No. of grid points	No. of time steps	CPU time, s Osher scheme	CPU time, s MacCormack method
VAX 11/780	21	400	18.41	9.99
VAX 11/780	21	1000	43.81	21.26
CDC 7600	31	1000	4.311	1.812

prescribing freestream quantities at all points and letting the body boundary conditions be fully felt even in the first step. Convergence from such a start is further proof of the robustness of the numerical procedure.

Contour lines of constant pressure obtained from the numerical results are plotted as solid lines in Fig. 5. The computational grid is also shown in this figure as a superimposed set of dashed lines. The crisp shock transition is clearly evident in this manner of portraying the results. Like the one-dimensional problems, the shock transition for this case, with the grid almost aligned with the shock, takes place in two points. In Fig. 6, we show the Mach number contours in increments of 0.2. The location of the shock as predicted by the shock "fit" calculation[18] (triangular symbols) is superimposed on the contours. Good agreement is evident, especially in view of the current first-order accuracy of our numerical procedure. A comparison of the surface pressure distribution between our results and the calculations of Lyubinov and Rusanov[18] is shown in Fig. 7. The sudden change in the pressure gradient seen at $\theta \simeq 45$ deg is due to an expansion shock of magnitude $\mathcal{O}(\Delta x)$ (order of accuracy of the method), well known for Godunov-type methods satisfying the entropy condition.[19] If the entropy condition is violated, the jump may be $\mathcal{O}(1)$. The velocity field about the circular cylinder is displayed in Figs. 8 and 9. The arrows shown represent the direction of flow by their orientation and the magnitude by their length. The arrows are drawn centered at the grid points. The sharp deceleration and deflection of the flow by the bow shock wave are clearly seen.

Computational Time

The Osher scheme is no more difficult to implement than any conventional scheme but obviously requires more operations. Computational times required to run the Osher scheme for the Laval nozzle problem were compared with the times required for MacCormack's method[20] for the same problem. The data are summarized in Table 2 and show that the first-order accurate Osher scheme is about twice as expensive as the second-order accurate MacCormack method.

Concluding Remarks

The Osher scheme is a novel finite difference method for solving hyperbolic systems of conservation laws. The application of the method to the two-dimensional Euler equations in general coordinate systems has been explained in this paper. The current treatment is explicit and first-order accurate. Research is already underway to develop second-order accurate and implicit versions of the algorithm.

Acknowledgments

This study was begun at the Rockwell International Science Center. It was further supported by NASA Langley Research Center under Grant NAG 1-269 awarded to Stanford University and Grant NAG 1-270 awarded to UCLA. Some computer time was provided by NASA Ames Research Center.

References

[1] Kutler, P., "Computation of Three-Dimensional, Inviscid Supersonic Flows," *Progress in Numerical Fluid Dynamics, Lecture Notes in Physics*, Vol. 41, 1975, pp. 287-374.

[2] Steger, J. L., "Implicit Finite-Difference Simulation of Flow About Arbitrary Two-Dimensional Geometries," *AIAA Journal*, Vol. 16, July 1978, pp. 679-686.

[3] Godunov, S. K., "A Finite-Difference Method for the Numerical Computation of Discontinuous Solutions of the Equations of Fluid Dynamics," *Matematicheskii Sbornik*, Vol. 47, 1959, pp. 271-290.

[4] van Leer, B., "Upwind Differencing for Hyperbolic Systems of Conservation Laws," ICASE Internal Report, Doc. 12, 1980.

[5] Steger, J. L. and Warming, R. F., "Flux Vector Splitting of the Inviscid Gasdynamic Equations with Applications to Finite Difference Methods," NASA TM 78605, 1979.

[6] Roe, P. L., "Approximate Riemann Solvers, Parameter Vectors, and Difference Schemes," *Journal of Computational Physics*, Vol. 43, 1981, pp. 357-372.

[7] Chakravarthy, S. R., Anderson, D. A., and Salas, M. D., "The Split-Coefficient Matrix Method for Hyperbolic Systems of Gas Dynamic Equations," AIAA Paper 80-0268, 1980.

[8] Chakravarthy, S. R., "Inviscid Analysis of Dual-Throat Nozzle Flows," AIAA Paper 81-1201, 1981.

[9] Chakravarthy, S. R., "Euler Equations—Implicit Schemes and Implicit Boundary Conditions," AIAA Paper 82-0228, 1982; *AIAA Journal*, Vol. 21, May 1983, pp. 699-706.

[10] Engquist, B. and Osher, S., "Stable and Entropy Satisfying Approximations for Transonic Flow Calculations," *Mathematics of Computation*, Vol. 36, 1981, pp. 321-352.

[11] Engquist, B. and Osher, S., "One Sided Difference Schemes and Transonic Flow," *Proceedings of National Academy of Sciences, USA*, Vol. 77, 1980, pp. 3071-3074.

[12] Engquist, B. and Osher, S., "One Sided Difference Equations for Nonlinear Conservation Laws," *Mathematics of Computation*, Vol. 36, 1981, pp. 321-352.

[13] Goorjian, P. M. and van Buskirk, R., "Implicit Calculations of Transonic Flow Using Monotone Methods," AIAA Paper 81-0331, 1981.

[14] Osher, S., "Numerical Solution of Singular Perturbation Problems and Hyperbolic Systems of Conservation Laws," *North Holland Mathematical Studies*, Vol. 47, 1981, pp. 179-205.

[15] Osher, S. and Solomon, F., "Upwind Schemes for Hyperbolic Systems of Conservation Laws," *Mathematics of Computation*, Vol. 38, 1982, pp. 339-377.

[16] Osher, S. and Chakravarthy, S. R., "Upwind Schemes and Boundary Conditions with Applications to Euler Equations in General Geometries," *Journal of Computational Physics*, to appear.

[17] Abrahamsson, L. and Osher, S., "Upwind Schemes for Flux Functions Depending on Independent and Dependent Variables," (in preparation).

[18] Lyubimov, A. N. and Rusanov, V. V., "Gas Flows Past Blunt Bodies," NASA-TT-F 715, Feb. 1973.

[19] Van Leer, B., "On the Relation Between the Upwind-Differencing Schemes of Godunov, Engquist-Osher, and Roe," *SIAM Journal of Scientific and Statistical Computing*, to be published.

[20] MacCormack, R. W., "The Effect of Viscosity in Hypervelocity Impact Cratering," AIAA Paper 69-354, 1969.